Fuel-cell grade hydrogen production by coupling steam reforming of ethanol and carbon monoxide removal

Bernay Cifuentes[1,3], Felipe Bustamante[1], Juan A. Conesa[2] and Martha Cobo[3]*

[1]Environmental Catalysis Laboratory, Department of Chemical Engineering, Universidad de Antioquia, Calle 67 No. 53 - 108, Medellín, Colombia.

[2]Department of Chemical Engineering, Universidad de Alicante, P.O. Box 99, Alicante E-03080, Spain.

[3]Energy, Materials, and Environment Laboratory, Department of Chemical Engineering, Universidad de La Sabana, Campus Universitario Puente del Común, Km. 7 Autopista Norte, Bogotá, Colombia.

*Corresponding author: Email: martha.cobo@unisabana.edu.co, Tel: +571 8615555 Ext. 25207, Fax: 571 8615555

Abstract

The integration of H_2 production and purification is an essential step in the development of sustainable power generation in proton exchange membrane fuel cells. Thence, coupling of steam reforming of ethanol (SRE) and carbon monoxide removal was evaluated for further hydrogen production in fuel cells. Firstly, SRE on $RhPt/CeO_2$-SiO_2 catalyst was carried out at 700 °C, displaying a stable product distribution for 120 h. Then, CO removal from the actual post-reforming stream was evaluated over several $AuCu/CeO_2$ catalysts with different Au:Cu weight ratios (1:0, 3:1, 1:1, 1:3, and 0:1). The role of each active metal was identified: Au favors CO conversion by the formation of carbon intermediates, and Cu improves CO_2 selectivity due to its redox properties. A 1:1 Au:Cu weight ratio on the $AuCu/CeO_2$ catalyst at 210 °C favors complete CO removal from the post-reforming stream, achieving fuel-cell grade hydrogen production. However, 25% of H_2 was loss during the CO removal step, which is very high compared to studies with synthetic feeds. These high H_2 loss would be the result of a complex network of reactions occurring during the real post-reforming cleaning. Characterization tests allowed us to identify that CeO_2, combined with the Cu redox properties, favors water decomposition and CO conversion. Likewise, catalyst reduction might favor Au-Cu alloy formation due to the similar crystal lattice. Finally, stability tests showed that $Au_{1.0}Cu_{1.0}/CeO_2$ catalyst is susceptible to rearrangement due to the cumulative oxidation of its surface during operation. Nonetheless, periodic *in-situ* reduction treatment contributes to the Au-Cu alloy formation and stabilization, maintaining high activity and mitigating H_2 loss. Indeed, $Au_{1.0}Cu_{1.0}/CeO_2$ catalyst was active for 95 h when reduced every 24 h, achieving fuel-cell grade hydrogen with a minimum of 14% H_2 loss.

Keywords: Bimetallic catalysts; Ceria; CO-PROX; Methanation; Water gas shift reaction.

1. Introduction

Hydrogen (H_2) is a promising fuel to develop a cleaner energy system because it can be used in fuel cells (FC) to decarbonizing simultaneously mobile and stationary applications [1]. Water, heat, and electricity are the only products in FC fed with H_2. Also, this technology can be integrated with local renewable resources to improve energy efficiency and security. For instance, H_2 can be obtained from fermentable biomass, which is widely present in industrial and agricultural wastes, allowing to close the CO_2 cycle [2].

The general process for energy production from biomass could be divided into four stages, as shown in Figure 1. Traditionally, these stages are considered separately and information of integrating processes is still missing. Bioethanol production is well-studied and depends strongly on the kind of the biomass fermented and the purifications steps, but ethanol and water are the main products expected. In H_2 production from bioethanol, steam reforming of ethanol (SRE) stands out for having higher H_2 yield compared to other alternatives as partial oxidation or oxidative steam reforming [3]. Depending on the operating conditions and catalysts, SRE yields different amounts of H_2, carbon monoxide (CO), carbon dioxide (CO_2), and methane (CH_4) [4]. Therefore, the purification of the H_2 stream is required but the purification process depends on the end-use of H_2, so this stage is usually studied independently from the SRE. Finally, FC represents a great opportunity to develop environmentally-friendly commercial devices. Among FC, proton exchange membrane FC (PEM-FC) are the most commercialized because they can operate in a wide range of temperatures with high efficiency [5], making them suitable for diverse applications. Also, recent energy and economic simulations in Aspen Plus software show the potential of coupling SRE and PEM-FC technologies [6,7]. As the presence of CO is highly undesirable in PEM-FC applications due to its deleterious effect on the cell electrodes, these studies

include several stages to remove CO. However, an experimental study that integrates directly SRE and PEM-FC have been not reported because CO-removal is a bulky step [8]. Therefore, removal of CO from the H_2 stream prior to its use in PEM-FC is a key aspect in implementing of this technology.

Figure 1

Table 1 shows the reactions that would be involved in CO-removal from H_2 streams, along with the main side-reactions. Conventionally, CO-removal from post-reforming streams is carried out by a partial conversion through water gas shift reaction (WGSR) (Eq. 1) to ensure an outlet CO content close to 2000-5000 ppm [9] -which may require two reactors-, followed by a final stage to ensure low CO (<10 ppm [10]) -which could also include several reactors-. Preferential oxidation of CO (CO-PROX, Eq. 2) and CO methanation (Eq. 3) are the most common methods used in the final stage [11]. Among them, CO-PROX ensures the low CO concentrations (< 10 ppm) [12,13] suitable for most PEM-FC. Nevertheless, excess in H_2 losses is common during the final stage by the presence of secondary reactions (Eq. 4 and 5). Therefore, the conventional H_2 purification is extremely complex and bulky, limiting the application of the existing H_2 production technology in mobile and small FC applications [8]. Thus, an integration of CO-removal process in the same reactor has been proposed recently [14], which would be promising for the development of new applications with PEM-FC. Accordingly, the challenge to integrate H_2 production and purification lies on finding a catalytic system that ensures an elevated H_2 production and a complete CO removal in the post-reforming streams, reducing the number of reactor units.

Table 1. Chemical reactions involved in the CO-removal of post-reforming streams

Reaction	Description	
$CO + H_2O \rightleftharpoons CO_2 + H_2$	Water gas shift reaction	Eq. 1
$2CO + O_2 \rightarrow 2CO_2$	Preferential oxidation of CO	Eq. 2
$CO + 3H_2 \rightleftharpoons CH_4 + H_2O$	CO methanation	Eq. 3
$2H_2 + O_2 \rightarrow 2H_2O$	H_2 oxidation	Eq. 4
$CO_2 + 4H_2 \rightleftharpoons CH_4 + 2H_2O$	CO_2 methanation	Eq. 5

In previous works, our group designed an active and stable catalyst for the SRE by assessing different supports (CeO_2, ZrO_2, and La_2O_3) [15] and Rh:Pt ratios [16], as well as a novel mixed Ce:Si support [17]. In particular, a RhPt/CeO_2-SiO_2 catalyst with 0.4 wt % Rh, 0.4 wt % Pt, and a Ce/Si molar ratio of 2 in the support yields a H_2-rich stream (71% of H_2, 18% of CO, 3% of CO_2, and 7% of CH_4), making it a promising material for mobile and stationary applications. Now, it is our intention to clean this stream (i.e., remove CO) to be able to connect it to a PEM-FC.

Mono- and bi-metallic Au and Cu have been reported as promising active metals in WGSR [14,18,19] and CO-PROX [20]. The support also plays an important role in catalyst performance for CO removal. For example, CeO_2 could be used because surface oxygen vacancies favor the adsorption of carbon species, which promote WGSR [21], CO-PROX [11], and methanation [22]. Therefore, Au-Cu supported on CeO_2 has been reported as a favorable catalyst for the complete removal of CO in synthetic post-reforming streams (containing CO, H_2, CO_2, and H_2O) [12]. However, product distribution depends strongly on temperature, feed composition, and active metal ratio [17]. Therefore, the challenge is to evaluate the CO-removal in an actual post-reforming stream and identify operational variables that promote high activity and stability, preventing H_2 losses.

This study aimed to evaluate a catalytic system for CO-free H_2 production that couples SRE and CO-removal reactors, looking forward to designing an in-line catalytic system to produce electricity in PEM-FC. SRE was carried out over a $RhPt/CeO_2$-SiO_2 catalyst previously reported [17], and $AuCu/CeO_2$ catalysts were evaluated for CO-removal. The effect of the Au:Cu ratio on activity and selectivity was studied. Stability tests in continuous operation were conducted in the coupled system and some strategies for catalyst reactivation were assessed. Characterization tests, such as Brunauer–Emmett–Teller (BET) surface area, X-ray photoelectron spectroscopy (XPS), transmission electron microscopy (TEM), and thermogravimetric analysis (TGA) were carried out to determine possible changes on the $AuCu/CeO_2$ catalysts structure during CO-removal from post-reforming streams.

2. Experimental

2.1 Catalyst synthesis

$RhPt/CeO_2$-SiO_2 catalyst for SRE was prepared according to previous report [17]. Firstly, the CeO_2-SiO_2 support was prepared by mixing $Ce(NO_3)_3 \cdot 6H_2O$ (99.5%, Alfa Aesar, USA) and SiO_2 (Merck, Germany), using water as solvent and achieving a Ce/Si molar ratio of 2. The support was dried at 105 °C for 24 h and calcined at 500 °C in a muffle for 4 h. Subsequently, aqueous solutions of rhodium (III) chloride hydrate ($RhCl_3 \cdot H_2O$) (Aldrich Chem. Co., USA) and chloroplatinic acid hexahydrate ($H_2PtCl_6 \cdot 6H_2O$) (Aldrich Chem. Co., USA) were using to load Rh and Pt metals on the support by incipient wetness co-impregnation, achieving 0.4 wt% of each noble metal (Rh and Pt). The metals-support mixture was dried at 105 °C for 24 h, calcined at 700 °C in a muffle for 2 h, and sieved ensuring particle sizes between 74 and177 μm.

Au-Cu/CeO_2 catalysts for CO removal were prepared with different Au:Cu weight ratios, as shown in Table 2, by a two-step procedure. Firstly, $HAuCl_4 \cdot 3H_2O$ (99.9%, Sigma Aldrich, USA) was dissolved in water and the pH of the solution was adjusted to 6 with NaOH (0.1 M); then, CeO_2 (labelled as "Ce") was added and heated to 80 °C under continuous stirring for 2 h [20]; the resulting slurry was filtrated, washed with water, and dried at 105 °C for 24 h. Afterwards, the required amount of $Cu(NO_3)_2 \cdot 3H_2O$ (99%, Sigma Aldrich, USA) was used as Cu precursor and loaded to the previous prepared Au/CeO_2 catalyst by incipient wetness impregnation [23]. The total metal loading (Au+Cu) was 2 wt% in all catalysts. Catalysts were dried at 100 °C for 24 h, calcined in muffle at 500 °C for 2 h, and sieved to ensure a particle size between 74 and 177 μm. These samples were labeled as "fresh" (F) catalysts. The prepared AuCu/CeO_2 catalysts were represented as Au_xCu_{2-x}/Ce (x= 0, 0.5, 1.0, 1.5, and 2.0), where x indicates Au loading (wt. %).

Table 2. AuCu/CeO_2catalysts evaluated in the CO removal from post-reforming streams

Sample[1,2]	Au (wt.%)	Cu (wt.%)	Au: Cu (wt-ratio)	Weight loss of used samples (%)[3]			
				Total	ΔT1	ΔT2	ΔT3
CeO_2 (Ce)	-	-	-	5.1	2.5	1.6	1.0
$Cu_{2.0}$/Ce	0	2.0	0:1	2.1	1.3	0.4	0.4
$Au_{0.5}Cu_{1.5}$/Ce	0.5	1.5	1:3	1.9	1.4	0.3	0.2
$Au_{1.0}Cu_{1.0}$/Ce	1.0	1.0	1:1	2.0	1.4	0.4	0.2
$Au_{1.0}Cu_{1.0}$/Ce (NR)	1.0	1.0	1:1	4.6	3.6	0.4	0.6
$Au_{1.0}Cu_{1.0}$/Ce (R)	1.0	1.0	1:1	2.3	2.0	0.2	0.1
$Au_{1.5}Cu_{0.5}$/Ce	1.5	0.5	3:1	1.7	0.9	0.3	0.5
$Au_{2.0}$/Ce	2.0	0	1:0	1.6	0.8	0.3	0.5

[1]Sub-cript in catalysts corresponds to the nominal metal loading.
[2]NR: no reactivated sample during stability tests, and R: reactivated sample during stability test by *in situ* reduction cycles.
[3]Measured by TGA. ΔT1: 80 – 250 °C, ΔT2: 250 – 600 °C, and ΔT3: 600 – 1000 °C.

2.2 Catalytic tests

SRE was carried out over a RhPt/CeO_2-SiO_2 catalyst in a fixed-bed reactor (ID of 12 mm) at 700 °C, atmospheric pressure, and under kinetic control (i.e., avoiding external and internal mass transfer limitations), according to the procedure described elsewhere [17]. The catalytic bed was made of 50 mg of RhPt/CeO_2-SiO_2 and 250 mg of inert quartz particles. RhPt/CeO_2-SiO_2 catalyst was reduced *in-situ* with 8% H_2/N_2 (300 mL/min) at 700 °C for 1 h. SRE was conducted at 6.4 ± 0.2 $L*g_{cat}^{-1}*min^{-1}$ of space velocity (SV) (GHSV=63,500 h^{-1}) to avoid mass transfer limitations in the system. The feed was 0.03 mL/min of synthetic bioethanol (water/ethanol with a stoichiometric molar ratio of 3). Before entering the reactor the feed was diluted in Ar to achieve 1.8 and 5.4 mol% of ethanol and water, respectively, in the inlet stream. The SRE catalytic stability test was conducted for 120 h time-on-stream (TOS) using the conditions described above. Steady state SRE product distribution was reached after 30 min (see Supplementary Material, Figure S1), achieving yields of 5.1 ± 0.2 for H_2, 1.3 ± 0.2 for CO, 0.2 ± 0.03 for CO_2, and 0.5± 0.03 for CH_4; furthermore, product distribution remained stable, indicating that SRE's product distribution over RhPt/CeO_2-SiO_2 would not be a relevant variable during the CO-removal in post-reforming streams.

When the SRE's product distribution was stable (i.e., after 30 min), the SRE output was directly connected to the CO removal reactor to carry out the catalytic evaluation of CO conversion in actual post-reforming streams. The effluent stream from SRE was mixed with dry air, to achieve a O_2/CO molar ratio of 0.9 ± 0.04 in the inlet of the CO removal reactor: O_2/CO ratio was selected based on preliminary tests (see Supplementary Material, Figure S2), where the 0.9 ratio favors the CO conversion and mitigates H_2 losses, similarly to results reported by [24]. Likewise, water in post-

reforming was not condensed because activity and selectivity were slightly improved above 180 °C by water presence (see Supplementary Material, Figure S3), in agreement with [23]. Catalytic tests were started at 300 °C and the temperature was decreased in 20 °C intervals until 60 °C (continuous sequence, 20 min at each temperature) in a plug flow reactor (ID=12 mm). External and internal mass transfer limitations was controlled as reported in [17]. The catalytic bed was made of 50 mg of catalyst sample (Au-Cu/Ce catalysts shown in Table 2) and 250 mg of inert quartz particles. A SV of 6.5 ± 0.2 $L*g_{cat}^{-1}*min^{-1}$ was used in the CO removal reactor. All catalysts samples were reduced *in-situ* with 8 mol% H_2/Ar at 300 °C for 1 h, degassed in Ar at 300 °C for 30 min, and stabilized in 10% air/Ar at 300 °C for 30 min. These samples were labeled as "reduced–oxidized" (R-O) catalysts. Samples used in catalytic evaluation were labeled as "used" (U) catalysts. CO-removal stability tests with several reactivation treatments were conducted on $Au_{1.0}Cu_{1.0}$/Ce at 210 °C for 95 h TOS. Specifically, reactivation treatment consisted in *in-situ* catalyst reduction with 8 mol% H_2/Ar at 300 °C for 1 h at intervals of 24 h; this treatment was selected after evaluating several methods to reactivate the catalyst (see Supplementary Material, Table S1). The sample used during the stability tests without reduction treatments was labeled as "NR", and the *in-situ* reduced sample as "R" catalyst.

The outlet products of the SRE and CO-removal reactors were measured on-line by gas chromatography (Perkin Elmer, USA). The GC was equipped with an Innowax column (30 m, 0.53 mm ID, Perkin Elmer, USA) connected to a flame ionization detector (FID) and a Carboxen 1010 plot column (30 m, 0.53 mm ID, Restek, USA) connected to a thermal conductivity detector (TCD), using Ar as carrier. This configuration allowed measuring CO, CO_2, H_2, CH_4, ethylene, and ethanol. Carbon elemental balances between inlet and outlet of each reactor were measured in all tests.

CO conversion (x_i) and yield for each detected product were calculated by Eqs. 6 and 7.

$$x_i = \frac{F_{i,inlet\ y} - F_{i,outlet\ y}}{F_{i,inlet\ y}} * 100 \qquad \text{Eq. 6}$$

$$Yield_i = \frac{F_{i,outlet\ CO-removal}}{C_{inlet\ SRE}} \qquad \text{Eq. 7}$$

Where $F_{i,inlet\ y}$ is the mole flow (mol/min) of species i (ethanol, H_2, CO, CH_4, or CO_2) entering to the reactor y (SRE or CO-removal) and $F_{i,outlet\ y}$ is the mole flow (mol/min) of unreacted species i detected by GC in the outlet of the corresponding reactor.

2.3 Catalytic characterization

The catalyst surface area was determined by the single-point BET surface method in a ChemBET Pulsar TPR/TPD unit (Quantachrome Instruments, Boynton Beach, FL, USA). 70 mg of samples were previously degassed in He (20 mL/min) at 120 °C for 1 h; surface area was measured with 30% N_2 /He (20 mL/min) as the adsorption gas, at liquid nitrogen temperature. The measurement was repeated until a deviation less than 5% was obtained.

XPS spectra of catalysts were obtained using an VG-Microtech Multilab electron spectrometer (Thermo-Scientific, Waltham, MA, USA) with a twin anode radiation source in the Mg Kα (1253.6 eV) constant energy analysis mode and an energy flow of 50 eV. The analysis chamber was maintained at 5.10×10^{-8} Pa. The C 1s line was set at 248.6 eV. The binding energy (BE) values were obtained with a precision of 0.2 eV using the Peak Fit program of the spectrometer control program.

TEM was carried out in a JEOL JEM-2010 microscope at 200 kV coupled to energy-dispersive X-ray spectroscopy (EDX, INCA Energy TEM100, Oxford Instruments, Abingdon, UK) with a Si(Li) detector, 30 mm^2 detection area, and 142 eV resolution. Samples were dispersed in ethanol by ultrasonic vibration and dropped on a carbon film-coated copper grid. The active metal particles were measured with ImageJ software. The mean particle diameter was calculated according to Eq. 8, where n_i is the number of particles and d_i is the particle diameter [25].

$$\bar{d}_p = \frac{\sum_i n_i d_i^3}{\sum_i n_i d_i^2} \qquad \text{Eq. 8}$$

TGA using a thermogravimetric analyzer (Mettler Toledo, Columbus, OH, USA) were performed to measure moisture, residues, and deposits on catalyst samples. Each sample (20 mg) was previously degassed in N_2 (20 mL/min) at 100 °C for 1 h and then heated from 30 to 1000 °C in air (5 °C/min, 100 mL/min flow rate). Weight loss reported for used samples includes the subtraction of the weight loss obtained in R-O samples.

3. Results and discussion

3.1. Activity and selectivity of AuCu/CeO_2 catalysts during CO-removal

Figure 2 shows CO conversion, H_2 loss, and CO_2 and CH_4 yield over AuCu/Ce catalysts between 60 and 300 °C; the feed is the post-reforming stream. At 210 °C, CeO_2 achieved a maximum of 55% CO conversion (Figure 2a) with 15% H_2 loss (Figure 2b). Moreover, CO_2 and CH_4 were produced at rates of 0.3 mol CO_2/mol CO inlet (Figure 2c) and 0.05 mol CH_4/mol CO inlet (Figure 2d). These results show that CeO_2 mainly promoted CO-PROX (Eq. 2) with small amounts of methanation (Eq. 3 and 5).

This behavior can be related to the support activation. In fact, H_2 decomposition and methanation are favored on catalysts with a reduced surface [22]. Oppositely, CO adsorbed (CO_{ad}) reacts with support's lattice oxygen available over unreduced surfaces, favoring CO oxidation and avoiding methanation [26]. In this work, all catalysts samples were reduced *in-situ* with H_2/Ar for 1 h, degassed in Ar for 30 min, and stabilized in air/Ar for 30 min. Thus, CeO_2 mostly promoted CO-removal by CO-PROX, but produces small amounts of CH_4 by methanation probably due to the H_2 pretreatment.

Figure 2.

Catalytic performance of AuCu/Ce catalysts with different Au:Cu weight ratios was evaluated in CO-removal of the post-reforming stream. A volcano-shape was observed in CO conversion with temperature (Figure 2a), due to the thermodynamic limitations of this reaction at high temperature. Besides, when Au loading increased, CO conversion was favored (Figure 2a) because Au is 9 times more active than Cu in WGSR (Eq. 1) and CO-PROX (Eq. 2) reactions [27]. Also, Au favors simultaneously CO and O_2 adsorption, reducing the activation energy of CO oxidation [12], and promotes changes in the surface of the catalyst, favoring CO oxidation [28]. Thus, Au inclusion on AuCu/Ce catalysts fosters CO removal by possible changes in the catalysts structure, as will be addressed below ("Catalysts characterization", Section 3.3).

Au:Cu ratio in the AuCu/Ce catalysts also affected H_2 losses, which is undesirable. Two zones were identified for H_2 losses on AuCu/Ce catalysts (Figure 2b). Between 60 and 175 °C H_2 losses increased with temperature, as expected [29]; catalysts with high Au content ($Au_{2.0}$/Ce, $Au_{1.5}Cu_{0.5}$/Ce, and $Au_{1.0}Cu_{1.0}$/Ce) showed the higher H_2 losses. Between 175 and 300 °C, on the other hand, H_2 losses tend

to decrease, mostly on $Au_{1.5}Cu_{0.5}$/Ce and $Au_{1.0}Cu_{1.0}$/Ce. Active sites for CO-PROX on Au/Ce is a combination of Au^0 and Au^+–OH^- species [30], where Au^0 activates O_2 molecules and OH^- groups provide the pathway for the CO_2 formation, which is an effective way to remove CO. Meanwhile, reduced Cu interacts directly with CO to form CO_2, helped by the near oxygen vacancies [31], ensuring high CO_2 selectivity of Cu/Ce. Thus, despite the Au mechanism is considered more effective to CO decomposition [27], the Cu mechanism could achieve lower H_2 losses because it does not involve H* species in the CO removal.

CO_2 yield on AuCu/Ce catalysts also displays different behavior with temperature, Figure 2c. Between 60 and175 °C, CO_2 yield increases with temperature, the change being more pronounced on $Cu_{2.0}$/Ce, $Au_{0.5}Cu_{1.5}$/Ce, and $Au_{1.0}Cu_{1.0}$/Ce. Decrease of CO_2 yield at higher temperatures maybe the result of a competition between CO and H_2 oxidation [32]. Figure 2d shows that the CH_4 formation is mainly promoted at intermediate temperatures (110-190 °C), especially on $Au_{2.0}$/Ce, $Au_{1.5}Cu_{0.5}$/Ce, and $Au_{1.0}Cu_{1.0}$/Ce. High CH_4 yield was not expected because Au- and AuCu-supported catalysts are recognized to avoid methanation during CO-PROX of synthetic post-reforming stream [27]. However, Wang at al. [31] evaluated Au-supported catalysts for CO-PROX, reporting both CO and CO_2 methanation at 160 °C, with 97% CO conversion on Au/Ce. Thus, AuCu/Ce catalysts could favor methanation under certain conditions. The H_2 loss profile matches that of CH_4 yield (Figure 2b and d). Accordingly, $Au_{1.0}Cu_{1.0}$/Ce catalyst showed the lower H_2 losses (25%, see Figure 2b) with complete CO conversion at 210 °C (see Figure 2a). However, H_2 losses are still elevated compared to the recommended goal (<5% [33]) for CO-PROX. Independent evaluation of WGSR, CO-PROX, CO-methanation, and CO_2-methanation on $Au_{1.0}Cu_{1.0}$/Ce catalyst (see Supplementary Material, Figure S4) revealed that CO removal on actual post-reforming stream is not a cumulative contribution of the CO-

removal reactions. The high CO concentration and the complex network of reactions in an actual post-reforming stream could favor H_2 losses greater than 5%. Thus, despite the high H_2 loss, CO-removal of post-reforming streams on $Au_{1.0}Cu_{1.0}$/Ce catalyst at 210 °C ensures FC-grade H_2. Therefore, stability tests were carried out to evaluate this FC-grade H_2 production, to identify the catalyst stabilization time, and to check the possible abrupt changes that could shift the behavior of the catalyst outside the narrow operation window observed in Figure 2.

3.2. Stability of the coupled SRE/CO-removal system

Catalysts stability and productivity are the most relevant industrial parameters [34]. So, these characteristics must be established prior to a catalyst extensive application. Thence, $Au_{1.0}Cu_{1.0}$/Ce catalyst was subjected to a stability tests at 210 °C. In preliminary tests (see Supplementary Material, Figure S5), $Au_{1.0}Cu_{1.0}$/Ce catalyst showed rapidly deactivation during 40 h TOS, accompanied by a high CH_4 production. Thus, several reactivation treatments were carried out (see Supplementary Material, Table S1 and Figure S5). An *in-situ* reduction (treatment 4 in Table S1) with 8 mol% H_2/Ar stream (300 mL/min) at 300 °C for 1 h followed by a degasification in Ar at 300 °C for 30 min was selected as treatment to avoid catalysts deactivation. Figure 3 shows the catalytic performance of the $Au_{1.0}Cu_{1.0}$/Ce catalyst undergoing the reactivation treatment every 24 h. Complete CO conversion was observed when the catalysts was periodically reduced (see Figure 3a), suggesting that a reduced catalyst surface is paramount in the CO removal. In fact, Au-Cu alloy formation [23] increases surface oxygen mobility [10] and improves the Cu redox properties [13], which are key factors to favor CO oxidation, whereas excessive surface oxidation by the presence of oxidants in the gas phase could quickly affect catalytic activity [10]. Thus, accumulative surface oxidation by O_2 and water could reduce the catalytic activity, requiring the reduction cycles.

Figure 3

H_2 loss (e.g., conversion) are also shown in Figure 3a. After 1 h, H_2 losses decreased rapidly, achieving 9% at 9 h, followed by increasing and decreasing intervals. However, after the first reduction treatment, H_2 conversion was kept lower than 14%. Bimetallic catalysts supported on CeO_2 tend to experience surface rearrangements under both reducing and oxidizing atmospheres [35], affecting the catalytic performance. These rearrangements have been linked to the modification in the number of oxygen vacancies [36] which are involved in the oxidation mechanism [31]. Figure 3b shows CO_2 and CH_4 yield with TOS and reactivation cycles. Decrease of CH_4 and increase of CO_2 production are observed at the same time than H_2 losses decrease. Thus, methanation activity of the catalyst declined with TOS; furthermore, CH_4 consumption was observed in the reduced sample, indicating that CH_4 decomposition or reverse methanation could be taking place. This behavior could explain the increasing CO_2 yield and the mitigation of H_2 losses with TOS. Indeed, CH_4 increased rapidly in N-R samples at 23 h TOS (see Supplementary Material, Figure S5). Caputo et al. [37] reported that the reduction process contributes to Cu redistribution and stabilization on CuO/CeO_2. Thus, TOS could favor a rearrangement on the catalyst surface, which reduces CH_4 formation and H_2 losses. Nonetheless, oxidant species such as O_2 and water could affect the catalyst activity and selectivity, favoring a rapid deactivation. Periodic *in-situ* reduction could mitigate this accumulative surface oxidation, achieving high activity with less H_2 losses.

In this way, BET surface area, XPS, TEM, EDX, and TGA analyses were employed to identify the changes in the catalytic structure of AuCu/Ce catalysts resulting from Au:Cu ratio and TOS, which would enlighten the phenomena that is occurring during the CO-removal of post-reforming streams.

3.3. Catalysts characterization

Possible rearrangements in the catalyst structure by the presence of Cu and Au, and the operating conditions, could explain the catalytic behavior of AuCu/Ce during the CO removal from post-reforming streams. Thus, textural and morphological properties of AuCu/Ce catalyst were studied by BET surface area, XPS, TEM, EDX, and TGA.

3.3.1 BET surface area

BET surface areas of AuCu/Ce catalysts are shown in Figure 4. Surface area of the catalysts which were activated by reduction-oxidation (R-O) increased with Cu content, reaching a maximum of 84 m^2/g_{cat} for $Cu_{2.0}$/Ce. Nagaraja et al. [38] found that the BET surface area started increasing with increase in Cu loading on Cu/MgO due to the formation of CuO, which may cause changes in the crystallinity of the support. However, the presence of a second metal in Cu catalysts would mitigate CuO formation [39]. Thus, Cu inclusion in AuCu/Ce catalysts could promote changes in CeO_2 crystallinity, causing an increase in their BET surface area. A direct relationship between catalytic activity and catalysts surface area was not detected in this study, but the high CO_2 selectivity found in Cu catalysts could be attributed to their larger specific surface areas due to a higher Cu dispersion [40], which increased the availability of oxygen vacancies. However, BET surface area decreased after use (U samples), mostly with high Cu loadings ($Au_{1.0}Cu_{1.0}$/Ce, $Au_{0.5}Cu_{1.5}$/Ce, and $Cu_{2.0}$/Ce), suggesting that these catalysts could be more susceptible to surface changes and formation of carbonaceous

deposits with TOS. Likewise, samples used in stability tests showed a higher decreasing in surface area, especially on NR samples, which showed a 13.6% BET area reduction. Therefore, the post-reformed atmosphere could be favoring changes in the surface area of the catalyst, which could be mitigated by periodic reduction cycles.

Figure 4.

3.3.2 XPS

Oxidation states of the elements on AuCu/Ce catalysts were evaluated by XPS. Figure 5 shows the XPS spectra of Cu, Au, and Ce in AuCu/Ce catalysts before (R-U) and after (U) CO-removal reaction. The amount of each species was determined by integration of each characteristic peak. In R-O catalysts (see Figure 5a), three oxidation states were identified in Cu $2p_{3/2}$: Cu^0 (931 eV [41]), Cu^+ (933 eV [42]), and Cu^{+2} (939 and 942 eV [43]). Most Cu species corresponded to Cu^0. The Cu^0/Cu proportion was slightly higher in $Au_{0.5}Cu_{1.5}$/Ce (0.52) and $Au_{1.0}Cu_{1.0}$/Ce (0.51), compared to $Cu_{2.0}$/Ce (0.46), indicating that Au favors Cu reduction (Cu was not detected by XPS on $Au_{1.5}Cu_{0.5}$/Ce, possibly because of the low Cu loading in this sample). Nonetheless, Cu^0 is not an active species for CO oxidation [44], so its presence indicates a loss of active sites. This explains the activity decrease when the Cu loading increased in the catalyst (see Figure 2a). In contrast, Cu^+ is the main active site in CO-PROX over Cu catalysts as a result of its strong association with ceria (Cu-O-Ce) [45] and the fact that it acts as a selective adsorption site for CO, promoting CO_2 formation [46]. Therefore, a certain amount of oxidized Cu (Cu^{+2}) sites is necessary to inhibit H_2 dissociation [46]. The Cu^+/Cu^{+2} ratio in AuCu/Ce decreased in the order: $Cu_{2.0}$/Ce (1.2) > $Au_{0.5}Cu_{1.5}$/Ce (0.9) >$Au_{1.0}Cu_{1.0}$/Ce (0.7). Elevated amounts of Cu^+ species on $Cu_{2.0}$/Ce and $Au_{0.5}Cu_{1.5}$/Ce could be linked to the superior CO_2 yield of these catalysts

(see Figure 2c and d). However, a Cu^{+2} species deficiency on these catalysts could be associated with a high H_2 oxidation compared to $Au_{1.0}Cu_{1.0}$/Ce (see Figure 2b at temperatures between 170 and 255 °C). Thus, $Au_{1.0}Cu_{1.0}$/Ce seems to have the right Cu^{+}/Cu^{+2} ratio to ensure high activity, with lower hydrogen loss.

Regarding Cu in U samples (Figure 5b), $Au_{1.0}Cu_{1.0}$/Ce and $Cu_{2.0}$/Ce catalysts showed an increase in Cu^0 and Cu^+ species, decreasing Cu^{+2} species. Even in $Au_{1.0}Cu_{1.0}$/Ce, the decrease was so drastic that Cu^{+2} was not detected. Hence, these catalysts could favor high CO_2 selectivity, but could be also susceptible to lose activity and promote high H_2 oxidation under operation. $Au_{0.5}Cu_{1.5}$/Ce showed an increase in Cu^{+2} at the expense of Cu^0 and Cu^+, which would favor activity, but is undesirable for CO_2 selectivity. The oxidation of Cu could be ascribed to the presence of oxidants as O_2 and water, and the diffusion of lattice oxygen to the surface [47].

Figure 5.

Figure 5c shows XPS spectra of Au 4f for fresh, R-O samples. The characteristic peak of Au^0 around 84 eV was observed. The shift to lower BE (~ 0.3 eV) could be associated with an increase in electron density by the presence of Cu [23]. Au^0 and $Au^{\delta+}$ could interact with CO_{ad}, but Au^0-CO_{ad} species are most reactive with O_2 [48]. It is expected that the Au-CeO_2 interaction involves a charge transfer, leading to Au oxidized species [49]. However, oxidized species as Au^+ (85 eV [23]) and Au^{+3} (86eV [49]) were not detected, indicating that Au have a slight interaction with CeO_2, which increases Au activity. In used samples (Figure 5d), no significant changes were observed and only Au^0 was detected. Thus, alterations in Au oxidation state by operation were not identified on AuCu/Ce catalysts.

Figures 5e and f show XPS spectra of Ce; symbols of V and U represent the spin−orbit coupling of $3d_{5/2}$ and $3d_{3/2}$, respectively, associated with Ce^{+3} and Ce^{+4} species. Deconvoluted peaks of V^0, V´, U^0, and U´ could be ascribed to Ce_2O_3 (Ce^{+3}), while V, V´´, V´´´, U, U´´, and U´´´ correspond to CeO_2 (Ce^{+4}) [50]. Ten peaks were observed in all AuCu/Ce catalysts, indicating that CeO_2 is partially reduced. Partial reduction of Ce^{+4} to Ce^{+3} generates oxygen vacancies, which dissociates CO_2 into CO_{ad} species [51], and favor oxygen mobility, which can act as an oxidizing agent [47]. Table 3 shows the relative atomic content of the main species on AuCu/Ce catalysts. The Ce^{+3}/Ce^{+4} ratio for AuCu/Ce catalysts increased with Cu loading, which could be linked to the incorporation of Cu species into the lattice of CeO_2 and Cu^+ formation [52]. Thus, high selectivity of AuCu/Ce catalysts with high Cu loading could be associated to a synergetic effect of the redox characteristics of Cu and CeO_2, which are associated to the presence of both Cu^+ and CeO_2 oxygen vacancies. In addition, small crystal size of CeO_2 is expected when vacancies increase on surface [53], which could be related to the increase in BET area with Cu content (Figure 4). Oxygen vacancies contribute to the CO_2 decomposition and lead to the re-oxidation of Cu^+ and Ce^{+3} [54]. Then, the amount of oxygen vacancies must be stable to keep the catalytic cycle. Ce^{+3}/Ce^{+4} ratio decreased in $Cu_{2.0}$/Ce and $Au_{0.5}Cu_{1.5}$/Ce, remained constant in $Au_{1.0}Cu_{1.0}$/Ce, and increased in $Au_{2.0}$/Ce and $Au_{1.5}Cu_{0.5}$/Ce, indicating that Cu promotes the oxidation of CeO_2 under operation. The slight Ce^{+3} formation under reaction conditions could be ascribed to the reductive features of Au [55]. Thus, $Au_{1.0}Cu_{1.0}$/Ce has favorable Cu and Au loadings to promote and retain oxygen vacancies on the catalysts.

Table 3. Relative atomic content of main species on AuCu/Ce catalysts from XPS

Catalyst	Ce^{+3}/Ce^{+4}		O/Ce			Cu/Ce (10^2)			Au/Ce (10^2)		
	R-O	U	R-O	U	E	R-O	U	E	R-O	U	E
$Cu_{2.0}/Ce$	0.9	0.7	2.2	3.2	2.0	10.1	9.2	5.5	0.0	0.0	0.0
$Au_{0.5}Cu_{1.5}/Ce$	0.7	0.6	1.2	2.2	2.0	8.2	6.1	4.1	1.0	1.1	0.4
$Au_{1.0}Cu_{1.0}/Ce$	0.6	0.6	2.9	3.7	2.0	6.1	2.8	2.7	1.0	1.2	0.9
$Au_{1.0}Cu_{1.0}/Ce$ (NR)		0.4		3.9			2.7			1.2	
$Au_{1.0}Cu_{1.0}/Ce$ (R)		0.6		3.3			5.9			1.2	
$Au_{1.5}Cu_{0.5}/Ce$	0.5	0.7	2.8	3.6	2.0	ND	ND	1.4	1.1	1.4	1.3
$Au_{2.0}/Ce$	0.5	0.6	3.6	3.5	2.0	0.0	0.0	0.0	1.4	1.5	1.7

NR: no reactivated sample during stability tests and R: reactivated sample during stability test by *in situ* reduction. E: expected value. ND: no detected.

Relative atomic content of Cu and Au on CeO_2 surface is shows in Table 3. Higher Cu contents –with respect to the expected values (E)– were observed, indicating that Cu was deposited preferentially on the CeO_2 surface. Meanwhile, Au content on the surface of R-O samples is near to the expected value for fresh catalysts, indicating that Au could be adsorbed into the CeO_2 bulk.

XPS of O (not shown) indicates the presence of three main species: O^{-2} related to the lattice oxygen in CeO_2 about 529 eV, surface oxygen, and surface OH^- species, both associated to the peak at 531 eV [49]. Surface oxygen (O_s) and OH^- groups play an important role in the catalytic activity and selectivity. O_s can react with CO in the gas phase or with the CO_{ad}, which are formed by decomposition of CO_2 over the oxygen vacancies, to produce CO_2 [18]. OH^- species are intermediates required to CO-PROX on Au catalysts [30]. In R-O samples, significant changes in O_s and OH^- species by Au:Cu ratio were not identified and, in average, a 21% of oxygen detected corresponded to O_s and OH^- species. However, in used samples the amount of O_s and OH^- species increased, especially when the Au loading

was higher than 1 wt%. Also, the relative amount of oxygen on the surface increased in all catalysts after reaction (see Table 3). Au is a recognized metal to promote OH^- formation [30], which could augment by water decomposition [23]. Despite the inclusion of OH^- groups is considered an effective way to CO decomposition in CO-PROX [27], the excess in OH^- species could promote high amount of carbon intermediates [56], which could be hydrogenated easily [57]. In fact, the presence of OH^- species has been linked to simultaneous WGSR and CO-methanation [57]. Therefore, the inclusion of Au in AuCu/Ce catalysts could favor the formation of OH^- species under reaction conditions, which increases the activity but could also affect the selectivity by hydrogenated carbon intermediates.

After TOS, NR sample (Table 3) shows an increase of the relative abundances of Cu^0 and Cu^{+2} by 2 and 14%, respectively, meanwhile Cu^+ decreases by 19% with respect to the R-O sample. These changes could explain the drastic reduction in selectivity observed after 23 h TOS over this samples and the deactivation after 40 h TOS (see Supplementary Material, Figure S5). Increase in Cu^{+2} species could be associated with an accumulative surface oxidation during operation [47]. In R sample, relative abundances of Cu^+ and Cu^{+2} increased by 24 and 7%, respectively, meanwhile Cu^0 decreased 14% respect to the R-O sample. Increase in Cu^+ and Cu^{+2} could simultaneously mitigate both H_2 oxidation and CH_4 formation, reducing H_2 loss, as observed in Figure 3a. H_2 pretreatment reduces Cu species [47], which could be undergoing subsequent partial oxidation during reaction. Thus, the *in-situ* reduction-oxidation pre-treatment proposed in this work could balance the amount of Cu^0, Cu^+, and CuO_x species on the catalyst.

Changes in Au oxidation states between R-O and samples evaluated in stability tests (NR and R) were not detected. Ce^{+3}/Ce^{+4} of NR decreased 33% while remained constant in R sample respect to R-O

sample (Table 3). Decrease in Ce^{+3}/Ce^{+4} is associated with the reduction of oxygen vacancies, indicating that catalytic surface is slightly being oxidized with TOS. Also, a loss in the number of oxygen vacancies could affect the activity, because of the modification of the catalyst capacity to oxidize [47]. Therefore, TOS could be promoting accumulative oxidation of the catalytic surface by the presence of oxidating species, reducing Cu^{+} and oxygen vacancies species, which are necessary for CO oxidation. However, proposed reduction cycles could avoid excessive surface oxidation, favoring high activity and improving selectivity.

3.3.3 TEM

Figure 6 shows the TEM micrographs and particle size distribution of AuCu/Ce catalysts. The average particle sizes obtained from the TEM analysis are listed in Table 4. As Cu may form irregular, highly dispersed particles [37], it was not clearly identified in TEM micrographs; moreover, there is not enough contrast between active particles and support. In R-O samples, average active particle diameter of Au increased with Cu loading, suggesting that Cu promotes Au agglomeration or alloy formation. Laguna et al. [12] reported that the presence of Cu^{+2} segregated on the surface avoids Au sintering. An appreciable amount of Cu^{+2} species were identified by XPS; so, the increase in active particles by the Cu presence could be ascribed to an alloy formation. In used samples (U), average active particle diameter increased with respect to R-O samples. This change is more significant when Cu loading decreased, which could be associated with Au enrichment on the surface, observed by XPS.

Figure 6.

On the other hand, interaction between active metals and support could be assessed by the evaluation of interplanar distances [17]. The typical interplanar distance of 0.30 nm associated to CeO_2 (100) and 0.27 nm to CeO_2 (111) [58,59] were identified in all AuCu/Ce samples (see Figure 6a, b, and c). These configurations have been linked to the formation of OH^- from water dissociation and the reduction of Ce^{+4} to Ce^{+3} [60]. Thus, the high O_s and OH^- species density on the surface of used AuCu/Ce catalysts detected by XPS may be the result of water decomposition on CeO_2. Interplanar sizes of 0.18 and 0.24 nm correspond to Cu (111) and Cu (200) [61]. Also, Wanget al. [62] linked 0.30 nm distance to Cu_2O (Cu^+) formation, which matches with Cu XPS spectra. However, this value is the same of the interplanar distance of CeO_2 (100), thus it was not possible to establish a clear difference between the two configurations by TEM. Cu (111) and Cu (200) configurations were identified in all samples (R-O, U, NR, and R), as presented in Table 4. Cu (111) promotes the adsorption of H_2O without dissociation, mitigating OH^- formation but also favoring oxidation of CO_{ad} to CO_2 [18]. For Au, spacing of 0.236 nm has been reported by (111) lattice planes [62]. Similar interplanar distance and configuration of Cu and Au could promote alloys. Au-Cu alloy formation could have interplanar spaces between 0.19 and 0.23 nm [23], which were observed in bimetallic AuCu/Ce catalysts (see Figure 6b), indicating a possible Au-Cu alloy formation on bimetallic AuCu/Ce catalysts. Bracey et al. [63] suggested the Au-Cu alloy formation and stabilization requires a reduction treatment. Therefore, H_2 pretreatment could favor the Au-Cu alloy formation in bimetallic AuCu/Ce samples, which could be related to changes in activity and product distribution in the bimetallic samples compared to the monometallic ones (Figure 2).

Table 4. Morphological characteristics of AuCu/Ce catalysts obtained from TEM

Catalysts	Metal average surface-area-weighted diameter (d_p, nm)[a]		Metal dispersion (%)[b]		Interplanar sizes (nm)
	R-O	U	R-O	U	
$Cu_{2.0}/Ce$	-	-	-	-	0.18, 0.24, 0.25, 0.27, 0.30, 0.34
$Au_{0.5}Cu_{1.5}/Ce$	4.87	4.78	22.6	23.0	0.18, 0.21, 0.24, 0.27, 0.30, 0.31
$Au_{1.0}Cu_{1.0}/Ce$	4.85	5.07	22.9	21.7	0.19, 0.20, 0.21, 0.25, 0.27, 0.30
$Au_{1.0}Cu_{1.0}/Ce$ (NR)	4.85	5.6	22.9	19.0	0.19, 0.20, 0.21, 0.25, 0.27, 0.30
$Au_{1.0}Cu_{1.0}/Ce$ (R)	4.85	5.2	22.9	25.2	0.19, 0.20, 0.21, 0.25, 0.27, 0.30
$Au_{1.5}Cu_{0.5}/Ce$	4.66	4.96	23.7	25.2	0.20, 0.21, 0.24, 0.27, 0.30, 0.31
$Au_{2.0}/Ce$	4.40	5.22	25.0	21.1	0.24, 0.23, 0.30, 0.31, 0.34

[a]Obtained from TEM. [b]Metal dispersion defined as $1.1/d_s$[64]. [c]Measured by TEM.

3.3.4 TGA

The amount of adsorbed and deposited species was evaluated by TGA. Table 2 shows the weight loss of used samples. To facilitate the analysis, the results were separated into three temperature regions: ΔT1: 80 - 250 °C for the loss of water and volatile compounds; ΔT2: 250 - 600 °C for less stable deposits; and, ΔT3: 600 - 1000 °C for more stable ones. CeO_2 showed the highest weight loss in all intervals, indicating that the support is susceptible to adsorb species and promote carbon deposition during operation. Active metals (Cu and Au) reduced this weight loss, stressing their role to avoid deactivation. Mitigation of stable deposits is most significant in bimetallic $Au_{0.5}Cu_{1.5}/Ce$ and $Au_{1.0}Cu_{1.0}/Ce$. The presence of possible Au-Cu alloys in theses samples, as discussed above, contributed to mitigate carbonaceous species [23]. The presence of carbon intermediates favors surface carbon during CO-PROX [65]. As discussed in previous sections, carbon intermediates were favored by OH^- species, which are formed on CeO_2 and Au. Thus, OH^- groups could contribute to the excess of carbon intermediates which could be hydrogenated to produce CH_4 or carbonaceous deposits. In NR sample, the amount of stable deposits increased drastically compared to U sample, which could be

related to the deactivation observed in this sample during stability test (see Figure S-5 in Supplementary Material). In contrast, R samples showed less deposits compared to U samples. Au-Cu alloy formation and stabilization under reduction cycles [63] could contribute to mitigate carbon deposition [23]. Therefore, stabilization of Au-Cu alloys by reduction treatment are required to avoid deactivation by deposits, which stems from carbon intermediates formed on CeO_2 and Au.

4. Conclusions

CO removal in an actual post-reforming stream over $AuCu/CeO_2$ catalysts with different Au:Cu ratios was investigated. Post-forming composition remained constant due to the stable $RhPt/CeO_2$-SiO_2 catalyst used during the SRE. This stream was subjected to the CO catalytic cleaning. It was found that Au presence in the $AuCu/CeO_2$ catalyst favors CO conversion, but affects CO_2 selectivity. $Au_{1.0}Cu_{1.0}/Ce$ catalyst showed the lowest H_2 lose (25%) with total CO elimination at 210 °C. However, H_2 loss is higher than that reported for synthetic feeds because a complex network of reactions is present in the real post-reforming stream cleaning.

Characterization tests allowed to identify that CeO_2 promotes OH^- formation from water and interacts mainly with Cu trough a synergetic effect of the redox properties. Au favors both, H_2 adsorption and OH^- formation, improving the catalytic activity. While Cu increases the catalyst surface area and promotes CO_2 formation, increasing the selectivity of catalysts. Likewise, the similar crystal lattice of Au and Cu could favor Au-Cu alloy formation, especially under reducing atmospheres. Also, an excess of carbon intermediates by OH^- presence, which are formed on Au, and a high CO concentration in post-reforming streams was responsible for both undesirable CH_4 formation and the presence of stable deposits on the catalyst. Finally, stability tests showed that $Au_{1.0}Cu_{1.0}/CeO_2$ catalyst is susceptible to

rearrangement and cumulative surface oxidation during operation. Moreover, periodic *in situ* reduction treatment contributes to the Au-Cu alloy formation and stabilization, maintaining high activity and reducing H_2 loss with time. $Au_{1.0}Cu_{1.0}$/Ce catalyst was active for 95 h TOS, when is reduced every 24 h, achieving fuel-cell grade hydrogen with a minimum of 14% H_2 loss. However, H_2 loss by oxidation and methanation is still high. Thus, currently modification in the composition and synthesis method of the catalysts are being planned to achieve complete CO removal and H_2 loss below 5%.

5. Acknowledgments

The authors are grateful to Colciencias (Francisco Jose de Caldas Found) and Universidad de La Sabana for the financial support of this work through the Project ING-163 (Colciencias contract 174-2016). The authors also acknowledge Universidad de Antioquia and Universidad de Alicante for their support to this project. B. Cifuentes acknowledges Colciencias for the doctoral scholarship (grant number 727-2015).

7. Author contributions

This work was developed in equal parts by Bernay Cifuentes, Felipe Bustamante, and Martha Cobo. Juan A. Conesa participated in the characterization of Au-Cu/CeO_2 catalysts through performing techniques such as TEM, EDX, and XPS. Nevertheless, all the authors contributed to the writing and review of this document.

8. Conflicts of interest

There are no conflicts of interest to declare.

9. References

[1] N.P. Brandon, Z. Kurban, Philos. Trans. R. Soc. London A Math. Phys. Eng. Sci. 375 (2017).

[2] R. Roldán, Int. J. Hydrogen Energy. 40 (2015) 2035–2046.

[3] W. Cai, F. Wang, E. Zhan, A. Vanveen, C. Mirodatos, W. Shen, J. Catal. 257 (2008) 96–107.

[4] D. Zanchet, J.B.O. Santos, S. Damyanova, J.M.R. Gallo, J.M. C. Bueno, ACS Catal. 5 (2015) 3841–3863.

[5] U. Lucia, Renew. Sustain. Energy Rev. 30 (2014) 164–169.

[6] U. Gardemann, M. Steffen, A. Heinzel, Int. J. Hydrogen Energy. 39 (2014) 18135–18145.

[7] I. Rossetti, M. Compagnoni, M. Torli, Chem. Eng. J. 281 (2015) 1036–1044.

[8] T. V. Choudhary, D.W. Goodman, Catal. Today. 77 (2002) 65–78.

[9] R.J. Farrauto, Chem. Eng. J. 238 (2014) 172–177.

[10] L. Ilieva, P. Petrova, G. Pantaleo, R. Zanella, L.F. Liotta, V. Georgiev, et al., Appl. Catal. B Environ. 188 (2016) 154–168.

[11] O. Pozdnyakova, D. Teschner, A. Wootsch, J. Kröhnert, B. Steinhauer, J. Catal. 237 (2006) 1–16.

[12] O.H. Laguna, W.Y. Hernández, G. Arzamendi, L.M. Gandía, M. a. Centeno, J. a. Odriozola, Fuel. 118 (2014) 176–185.

[13] Q. Zhang, L. Shore, R.J. Farrauto, Int. J. Hydrogen Energy. 37 (2012) 10874–10880.

[14] T.R. Reina, S. Ivanova, O.H. Laguna, M.A. Centeno, J.A. Odriozola, Appl. Catal. B Environ.

197 (2016) 67–72.

[15] B. Cifuentes, M.F. Valero, J. a. J. Conesa, M. Cobo, Catalysts. 5 (2015) 1872–1896.

[16] B. Cifuentes, M. Figueredo, M. Cobo, Catalysts. 7 (2017) 15.

[17] B. Cifuentes, M. Hernández, S. Monsalve, M. Cobo, Appl. Catal. A Gen. 523 (2016) 283–293.

[18] O. Jakdetchai, T. Nakajima, J. Mol. Struct. THEOCHEM. 619 (2002) 51–58.

[19] C. Ratnasamy, J.P. Wagner, Catal. Rev. 51 (2009) 325–440.

[20] L.F. Córdoba, A. Martínez-Hernández, Int. J. Hydrogen Energy. 40 (2015) 16192–16201.

[21] N.K. Gamboa-Rosales, J.L. Ayastuy, M.P. González-Marcos, M.A. Gutiérrez-Ortiz, Catal. Today. 176 (2011) 63–71.

[22] D.C. Upham, A.R. Derk, S. Sharma, H. Metiu, E.W. McFarland, T. Onishi, et al., Catal. Sci. Technol. 5 (2015) 1783–1791.

[23] X. Liao, W. Chu, X. Dai, V. Pitchon, Appl. Catal. B Environ. 142–143 (2013) 25–37.

[24] Y. Choi, H.G. Stenger, J. Power Sources. 129 (2004) 246–254.

[25] N. Krishnankutty, M.A. Vannice, J. Catal. 155 (1995) 312–326.

[26] H.-H. Liu, Y. Wang, A.-P. Jia, S.-Y. Wang, M.-F. Luo, J.-Q. Lu, Appl. Surf. Sci. 314 (2014) 725–734.

[27] J. da S.L. Fonseca, H.S. Ferreira, N. Bion, L. Pirault-Roy, M. do C. Rangel, D. Duprez, et al., Catal. Today. 180 (2012) 34–41.

[28] T.R. Reina, C. Megías-Sayago, A.P. Florez, S. Ivanova, M.Á. Centeno, J.A. Odriozola, J. Catal.

326 (2015) 161–171.

[29] X. Chen, J.J. Delgado, J.M. Gatica, S. Zerrad, J.M. Cies, S. Bernal, J. Catal. 299 (2013) 272–283.

[30] T. Sakwarathorn, A. Luengnaruemitchai, S. Pongstabodee, J. Ind. Eng. Chem. 17 (2011) 747–754.

[31] H. Wang, H. Zhu, Z. Qin, G. Wang, F. Liang, J. Wang, Catal. Commun. 9 (2008) 1487–1492.

[32] H.C. Lee, D.H. Kim, Catal. Today. 132 (2008) 109–116.

[33] R.J.B. M. J. Kahlich, H.A. Gasteiget, Iournal New Mater. Electrochem. Syst. 1 (1998) 39–46.

[34] P. Lanzafame, G. Centi, S. Perathoner, Catal. Today. 234 (2014) 2–12.

[35] N.J. Divins, I. Angurell, C. Escudero, V. Pérez-Dieste, J. Llorca, Science (80-.). 346 (2014) 620–623.

[36] M. Ozawa, M. Haneda, M. Hattori, IOP Conf. Ser. Mater. Sci. Eng. 18 (2011) 182010.

[37] T. Caputo, L. Lisi, R. Pirone, G. Russo, Appl. Catal. A Gen. 348 (2008) 42–53.

[38] B.M. Nagaraja, A.H. Padmasri, B. David Raju, K.S. Rama Rao, J. Mol. Catal. A Chem. 265 (2007) 90–97.

[39] J. Chen, W. Li, R. Shen, Korean J. Chem. Eng. 33 (2016) 500–506.

[40] G. Landi, P.S. Barbato, A. Di Benedetto, L. Lisi, Appl. Catal. B Environ. 181 (2016) 727–737.

[41] J. Deng, L. Zhang, H. Dai, H. He, C.T. Au, Appl. Catal. B Environ. 89 (2009) 87–96.

[42] V. Hayez, A. Franquet, A. Hubin, H. Terryn, Surf. Interface Anal. 36 (2004) 876–879.

[43] E.B. Fox, A.F. Lee, K. Wilson, C. Song, Top. Catal. 49 (2008) 89–96.

[44] M. Tada, R. Bal, X. Mu, R. Coquet, S. Namba, Y. Iwasawa, Chem. Commun. (Camb). 2 (2007) 4689–4691.

[45] E. Moretti, M. Lenarda, L. Storaro, A. Talon, R. Frattini, S. Polizzi, et al., Appl. Catal. B Environ. 72 (2007) 149–156.

[46] C.S. Polster, H. Nair, C.D. Baertsch, J. Catal. 266 (2009) 308–319.

[47] S. Poulston, P.M. Parlett, P. Stone, M. Bowker, Surf. Interface Anal. 24 (1996) 811–820.

[48] S. Chen, L. Luo, Z. Jiang, W. Huang, ACS Catal. 5 (2015) 1653–1662.

[49] S. Zhang, X. Li, B. Chen, X. Zhu, C. Shi, A. Zhu, ACS Catal. (2014).

[50] D.M. Gu, Y.Y. Chu, Z.B. Wang, Z.Z. Jiang, G.-P. Yin, Y. Liu, Appl. Catal. B Environ. 102 (2011) 9–18.

[51] E.J. Choi, Y.H. Lee, D.W. Lee, D.J. Moon, K.Y. Lee, Mol. Catal. 434 (2017) 146–153.

[52] J. Wang, L. Zhong, J. Lu, R. Chen, Y. Lei, K. Chen, et al., 443 (2017) 241–252.

[53] G.W. Graham, W.H. Weber, C.R. Peters, R. Usmen, J. Catal. 130 (1991) 310–313.

[54] X. Gong, B. Liu, B. Kang, G. Xu, Q. Wang, C. Jia, et al., Mol. Catal. 436 (2017) 90–99.

[55] J.A. Hernández, S.A. Gómez, T.A. Zepeda, J.C. Fierro-González, G.A. Fuentes, ACS Catal. 5 (2015) 4003–4012.

[56] X. Wang, J.A. Rodriguez, J.C. Hanson, D. Gamarra, A. Martínez-Arias, M. Fernández-García, et al., J. Phys. Chem. B. 110 (2006) 428–434.

[57] S.H. Kim, S.W. Nam, T.H. Lim, H.I. Lee, Appl. Catal. B Environ. 81 (2008) 97–104.

[58] E.M. Slavinskaya, R.V. Gulyaev, A.V. Zadesenets, O.A. Stonkus, V.I. Zaikovskii, Y. V. Shubin, et al., Appl. Catal. B Environ. 166–167 (2015) 91–103.

[59] J. Malleshappa, H. Nagabhushana, B.D. Prasad, S.C. Sharma, Y.S. Vidya, K.S. Anantharaju, Opt. - Int. J. Light Electron Opt. 127 (2016) 855–861.

[60] D.R. Mullins, P.M. Albrecht, T.-L. Chen, F.C. Calaza, M.D. Biegalski, H.M. Christen, et al., J. Phys. Chem. C. 116 (2012) 19419–19428.

[61] C. Ping, F. Li, Z. Jian, J. Wei, Propellants, Explos. Pyrotech. 31 (2006) 452–455.

[62] Z. Wang, S. Zhao, S. Zhu, Y. Sun, M. Fang, CrystEngComm. 13 (2011) 2262.

[63] C.L. Bracey, P.R. Ellis, G.J. Hutchings, Chem. Soc. Rev. 38 (2009) 2231.

[64] R.M. Heck, R.J. Farrauto, S.T. Gulati, Third Edit, Wiley, 2009.

[65] G. Marbán, I. López, T. Valdés-Solís, Appl. Catal. A Gen. 361 (2009) 160–169.

Figures caption

Figure 1. The general process for energy production from biomass

Figure 2. (a) CO conversion, (b) H_2 loss, (c) CO_2 and (d) CH_4 yield for CO removal of a post-reforming stream on $AuCu/CeO_2$ catalysts. Inlet stream: 7.8% H_2, 2.0% CO, 0.5% CO_2, 0.3% CH_4, 1.4% H_2O, 1.8% O_2, 6.8% N_2, and 79.4% Ar. Total metal loading (Au+Cu) = 2 wt% in all catalysts.

Figure 3: (a) CO and H_2 conversion, and (c) CO_2 and (d) CH_4 yield during the CO removal of a post-reforming stream over $Au_{1.0}Cu_{1.0}/Ce$ catalysts. Intel stream: 7.8% H_2, 2.0% CO, 0.5% CO_2, 0.3% CH_4, 1.4% H_2O, 1.8% O_2, 6.8% N_2, and 79.4% Ar. Reaction conditions: SV=6.5 ± 2 $L*g_{cat}^{-1}*min^{-1}$; 50 mg of catalyst and 250 mg of inert quartz; 210 °C. Vertical lines show reactivation treatments every 24 h with an *in-situ* reduction with 8 mol% H_2/Ar (300 mL/min) at 300 °C for 1 h followed by degassing in Ar at 300 °C for 30 min.

Figure 4. BET surface area of $AuCu/CeO_2$ catalyst samples: after reduction-oxidation(R-O), use (U), stability without *in-situ* reduction treatment (NR), and stability with *in-situ* reduction treatment (R).

Figure 5. XPS spectra of Cu 2p (a and b), Au 4f (c and d), and Ce 3d (e and f) for reduced-oxidized (R-O) and used (U) samples of $AuCu/CeO_2$catalysts.

Figure 6. TEM images of reduced-oxidized (a) $Cu_{2.0}/Ce$, (b) $Au_{1.0}Cu_{1.0}/Ce$, and (c) $Au_{2.0}/Ce$ catalysts, and (d-g) particle size distribution histograms for reduced-oxidized and used $AuCu/CeO_2$ catalysts.

Figures

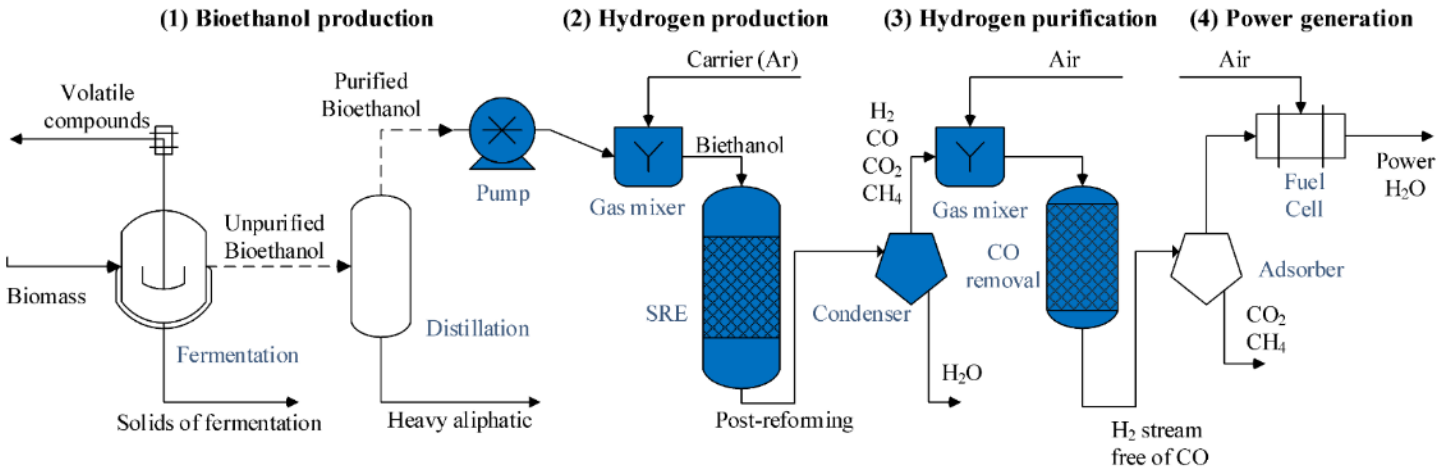

Figure 1.

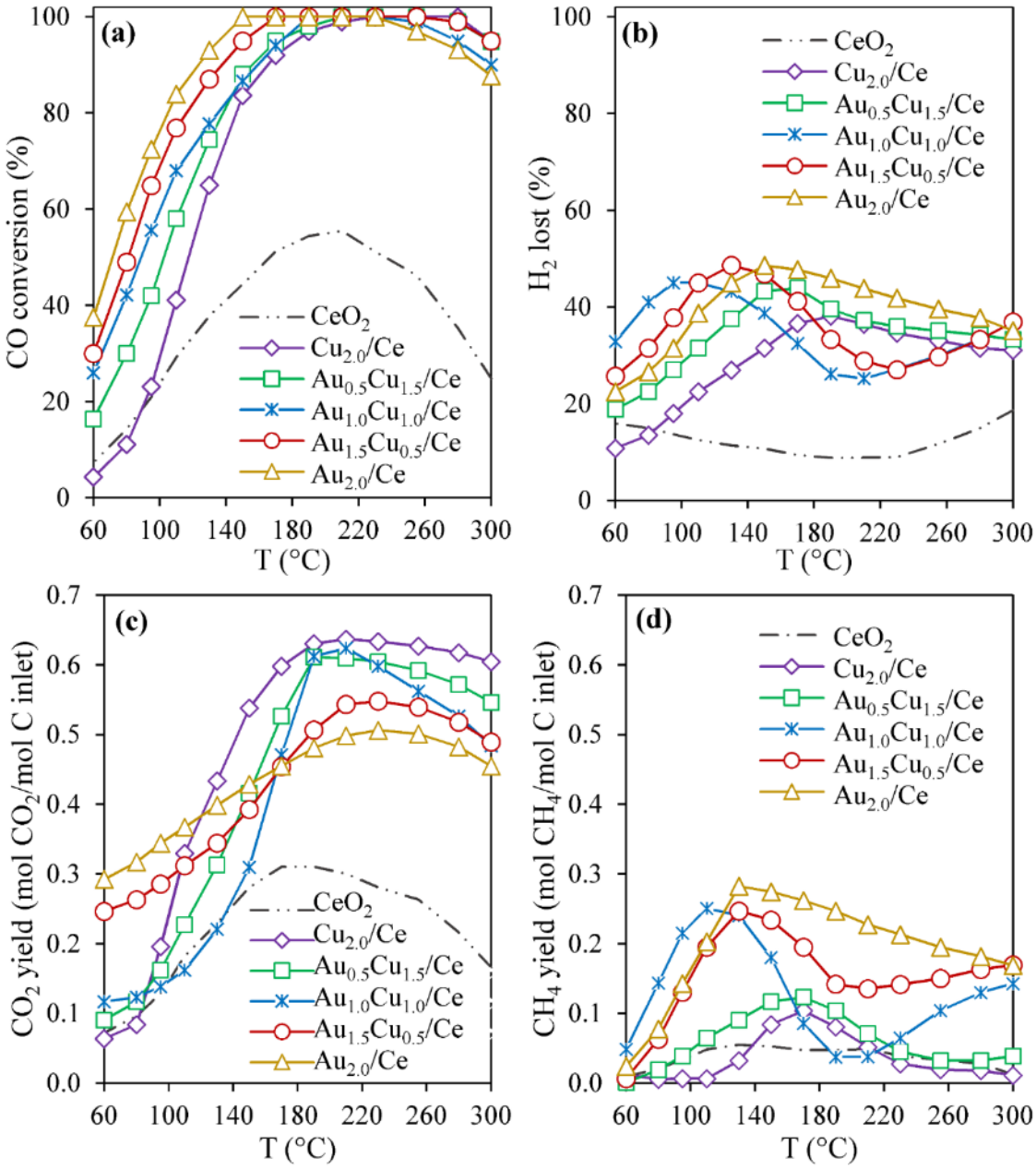
(a)
CO conversion (%)
T (°C)
(b)
H2 lost (%)
T (°C)
(c)
CO2 yield (mol CO2/mol C inlet)
T (°C)
(d)
CH4 yield (mol CH4/mol C inlet)
T (°C)
CeO2
Cu2.0/Ce
Au0.5Cu1.5/Ce
Au1.0Cu1.0/Ce
Au1.5Cu0.5/Ce
Au2.0/Ce

Figure 2.

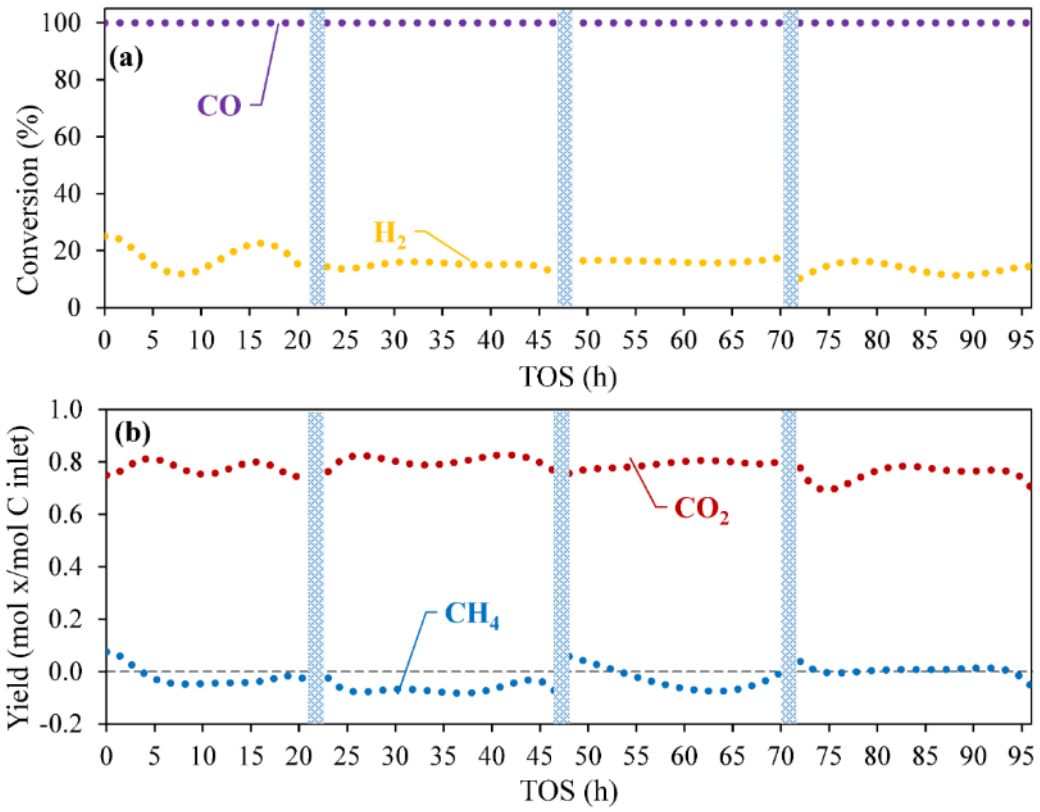

Figure 3.

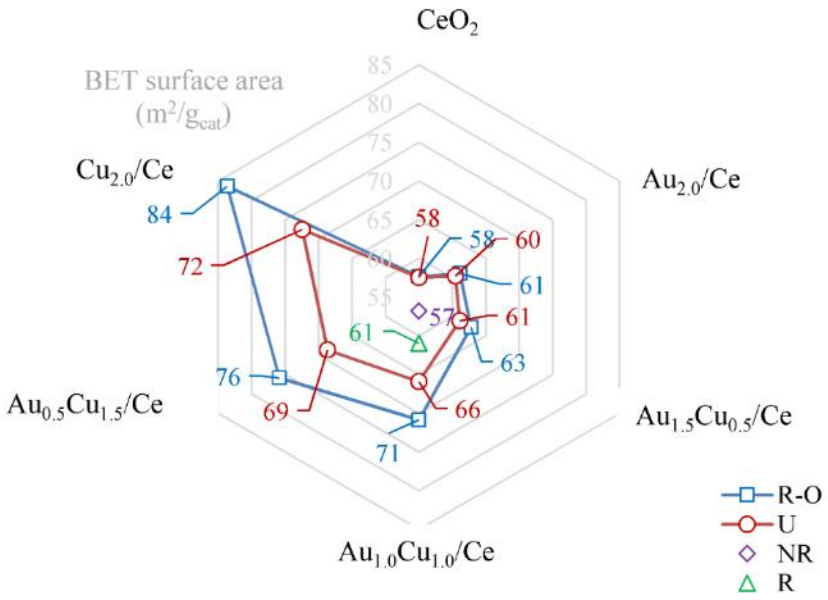
CeO2
BET surface area
(m2/gcat)
85
80
75
70
65
60
55
Cu2.0/Ce
Au2.0/Ce
Au0.5Cu1.5/Ce
Au1.5Cu0.5/Ce
Au1.0Cu1.0/Ce
84
72
58
58
60
61
57
61
61
63
76
69
66
71
R-O
U
NR
R

Figure 4.

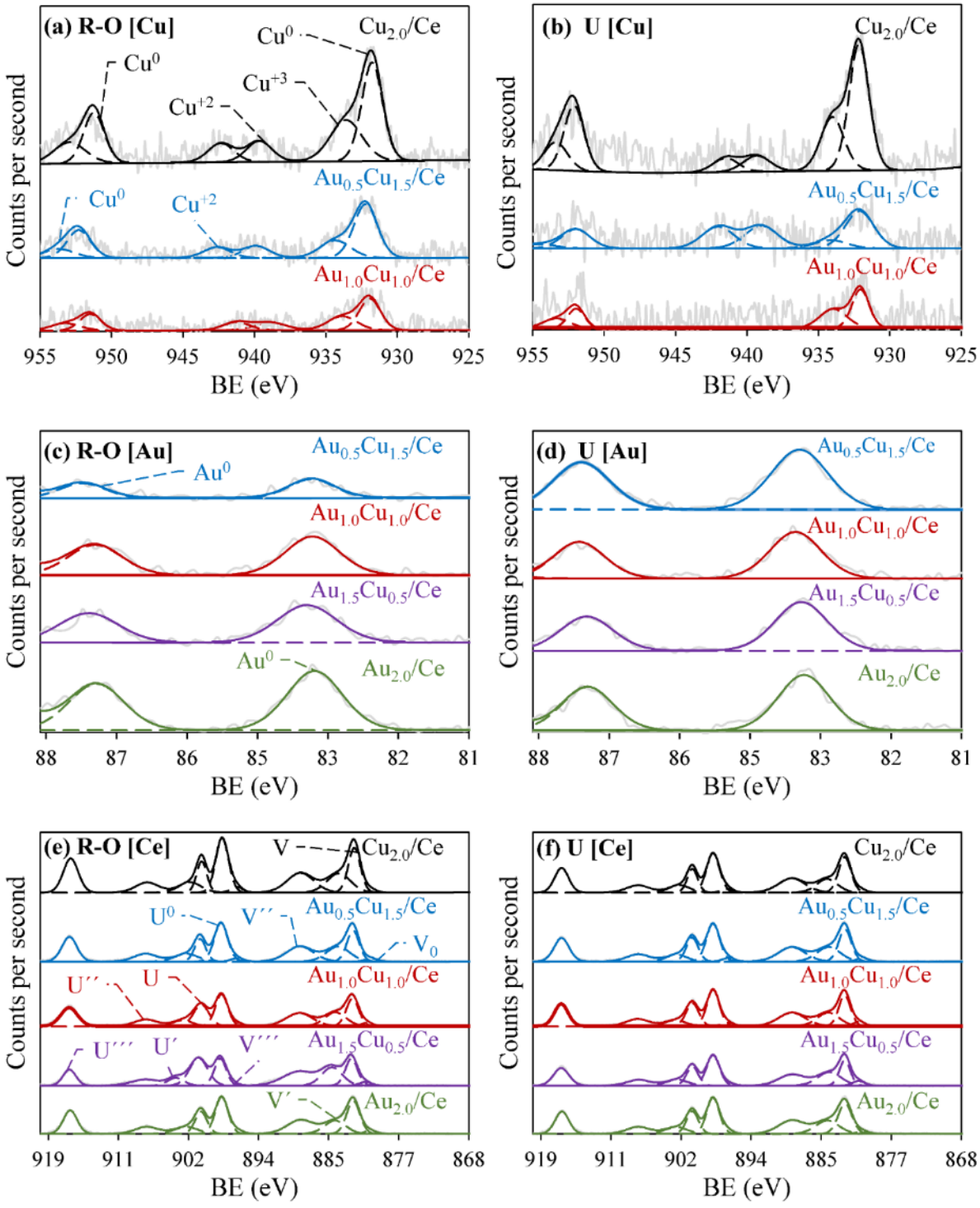
(a) R-O [Cu]
Cu0
Cu2.0/Ce
Cu0
Cu+3
Cu+2
Au0.5Cu1.5/Ce
Cu0
Cu+2
Au1.0Cu1.0/Ce
Counts per second
955 950 945 940 935 930 925
BE (eV)
(b) U [Cu]
Cu2.0/Ce
Au0.5Cu1.5/Ce
Au1.0Cu1.0/Ce
Counts per second
955 950 945 940 935 930 925
BE (eV)
(c) R-O [Au]
Au0.5Cu1.5/Ce
Au0
Au1.0Cu1.0/Ce
Au1.5Cu0.5/Ce
Au0
Au2.0/Ce
Counts per second
88 87 86 85 83 82 81
BE (eV)
(d) U [Au]
Au0.5Cu1.5/Ce
Au1.0Cu1.0/Ce
Au1.5Cu0.5/Ce
Au2.0/Ce
Counts per second
88 87 86 85 83 82 81
BE (eV)
(e) R-O [Ce]
V
Cu2.0/Ce
U0
V''
Au0.5Cu1.5/Ce
V0
U''
U
Au1.0Cu1.0/Ce
U'''
U'
V'''
Au1.5Cu0.5/Ce
V'
Au2.0/Ce
Counts per second
919 911 902 894 885 877 868
BE (eV)
(f) U [Ce]
Cu2.0/Ce
Au0.5Cu1.5/Ce
Au1.0Cu1.0/Ce
Au1.5Cu0.5/Ce
Au2.0/Ce
Counts per second
919 911 902 894 885 877 868
BE (eV)

Figure 5.

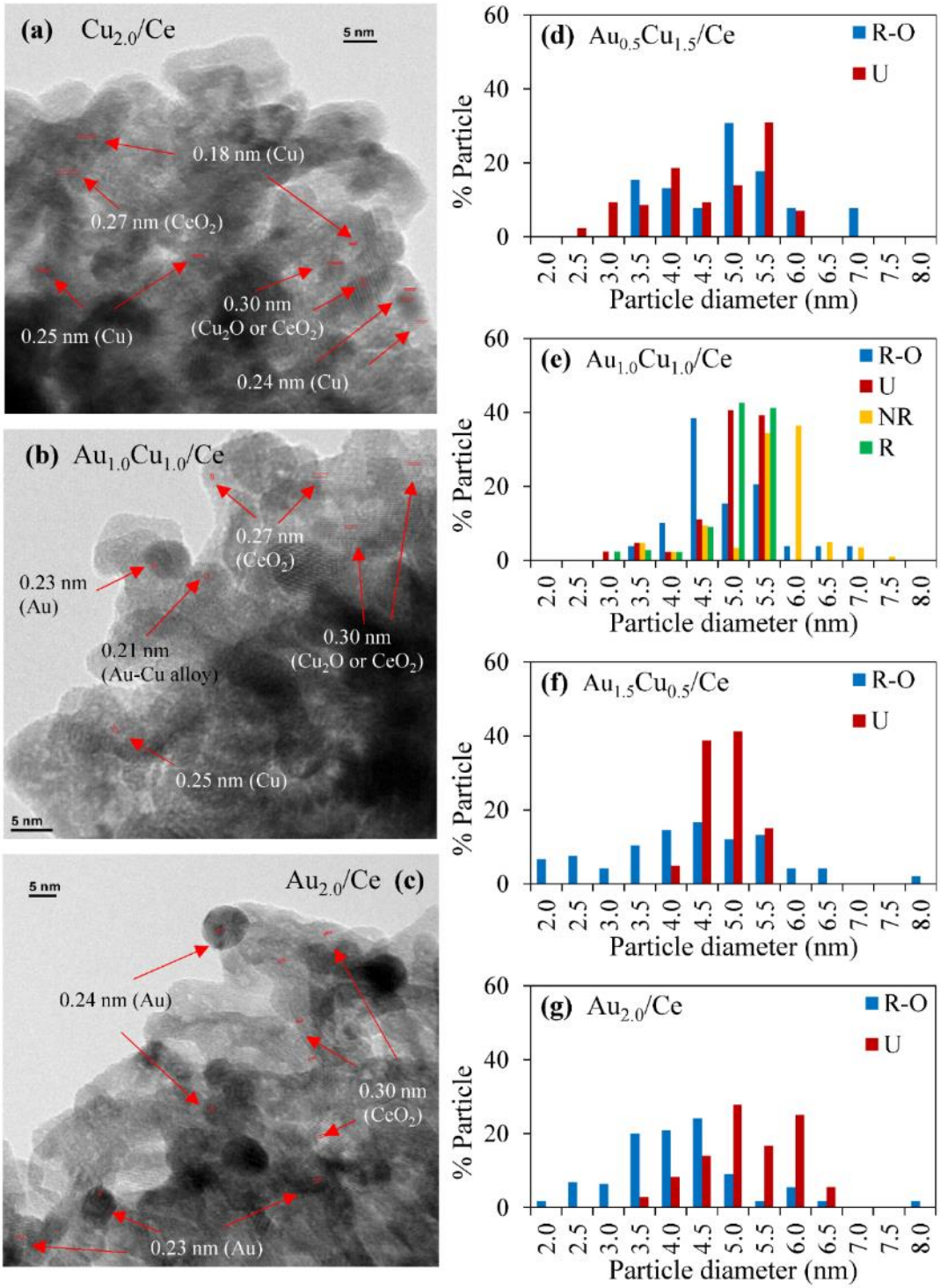
(a) Cu2.0/Ce
5 nm
0.18 nm (Cu)
0.27 nm (CeO2)
0.30 nm (Cu2O or CeO2)
0.25 nm (Cu)
0.24 nm (Cu)
(b) Au1.0Cu1.0/Ce
0.27 nm (CeO2)
0.23 nm (Au)
0.21 nm (Au-Cu alloy)
0.30 nm (Cu2O or CeO2)
0.25 nm (Cu)
5 nm
5 nm
Au2.0/Ce (c)
0.24 nm (Au)
0.30 nm (CeO2)
0.23 nm (Au)
(d) Au0.5Cu1.5/Ce
R-O
U
% Particle
Particle diameter (nm)
(e) Au1.0Cu1.0/Ce
R-O
U
NR
R
% Particle
Particle diameter (nm)
(f) Au1.5Cu0.5/Ce
R-O
U
% Particle
Particle diameter (nm)
(g) Au2.0/Ce
R-O
U
% Particle
Particle diameter (nm)

Figure 6.